WOOD RESEARCH doi.org/10.37763/wr.1336-4561/67.4.582597
e-ISSN 2729-8906
67(4): 2022 582-597 pp.

STUDY ON THE TIME-FREQUENCY CHARACTERISTICS AND PROPAGATION LAW OF ACOUSTIC EMISSION LONGITUDINAL WAVES IN WOOD GRAIN DIRECTION

SAIYIN FANG[1], MING LI[2,3], TINGTING DENG[1], KUN DU[1]

[1]SOUTHWEST FORESTRY UNIVERSITY, CHINA
[2]KEY LABORATORY OF ADVANCED PERCEPTION AND INTELLIGENT CONTROL OF HIGH-END EQUIPMENT OF MINISTRY OF EDUCATION, CHINA
[3]ANHUI POLYTECHNIC UNIVERSITY, CHINA

(RECEIVED DECEMBER 2021)

ABSTRACT

To study the propagation law of acoustic emission (AE) longitudinal waves in wood, the relationship among wave velocity, standing wave fundamental frequency and Young's modulus of elasticity was studied, and the energy decay model of AE longitudinal waves along the grain direction was established. Firstly, the propagation velocity of the longitudinal wave was calculated using the time-difference method. Then, the relationship between the wave velocity and Young's modulus of elasticity was analyzed and the method of calculating the longitudinal wave velocity using the fundamental frequency was proposed. Finally, using different levels' pulse strings as AE sources, the attenuation law of AE signal energy with distance was studied. The results show that the longitudinal wave velocity can be estimated more accurately by using the standing wave fundamental frequency. The influence of Poisson's ratio needs to be considered when calculating the Young's modulus of elasticity by using the longitudinal wave velocity.

KEYWORDS: AE longitudinal waves, standing fundamental frequency, Young's modulus of elasticity, Poisson's ratio, AE energy attenuation.

INTRODUCTION

The material transitions to a low-energy steady state by releasing strain energy during the damage process. This phenomenon of releasing strain energy in the form of stress waves is also known as acoustic emission (AE), and this active release of AE signal has become the basis

for dynamic non-destructive testing (NDT) of materials. The application of AE technology in wood NDT is becoming increasingly widespread. (Niemz et al. 2009, Nasir et al. 2020, Krauss et al. 2011, Contea et al. 2015).

Berg et al. (2000) investigated the fracture process of wood at different temperatures, moisture contents and loading directions by monitoring the AE behavior during the wood compression process, and the results showed that the elastic modulus, compressive strength and the cumulative number of AE events all tended to decrease with the temperature increased. Reiterer et al. (2000) investigated the AE behavior of the type I fracture process by wood splitting tests. AE parameters mainly included number of AE events, amplitude and frequency spectrum. The results showed that the AE count of conifer wood was much higher before reaching the maximum stress. Aicher et al. (2001) used AE analysis to study the damage evolution of spruce during vertical fiber direction stretching, and the results showed that these local damages could be accurately traced in space and time by AE source location analysis. Chen et al. (2006) studied the AE phenomenon during torsional fracture of wood and showed that AE activity occurred in all specimens before the appearance of macroscopic cracks, and the results indicated that more AE events occurred in broadleaf wood, but the number of AE events in coniferous specimens was higher than in broadleaf specimens after macroscopic cracks produced. Ohuchi et al. (2011) monitored AE activity in compact tensile specimens of Japanese cedar with different cracking systems and found that AE detection was more sensitive to type I fracture in the TR system. Lamy et al. (2015) tested for Douglas-fir double-cantilever beam type I fracture, and the results showed that AE testing was more advantageous as a fully autonomous monitoring method in monitoring the crack sprouting and extension process. It was also pointed out that based on obtaining sufficient AE information, the AE source localization method is very effective for studying fracture mechanisms such as fracture process zones or crack bridging. Similar literature reports can be found in the work of Wu et al. (2014), and Yang et al. (2017). Nasir V et al. (2019) applied AE sensors to collect stress wave data and created a neural network model to classify thermal modified materials. Sun et al. (2006) proposed that the cumulative number of AE events and the rate of increase of accumulated energy can be used to distinguish the different states of wood under stress conditions, while the AE incidence, rise time, and amplitude parameters can be used to predict two "tipping points" when the material starts to fracture in the dangerous phase and when a large number of fibers fracture in the severe dangerous phase. Shao et al. (2009) found that some low-amplitude AE signals were generated at the beginning of the three-point bending test loading, while a large number of high-amplitude AE signals appeared near the peak load and at the ductile fracture stage. Guo et al. (2011) showed that the amplitude, effective voltage, accumulated energy, total ring count and other parameters of AE signals can effectively characterize the internal damage evolution process of wood matrix composites. Li et al. (2018) conducted a series of studies on wood AE signal waveform, using methods such as wavelet processing and empirical mode decomposition to reconstruct AE signal waves from the original signals, and then used signal correlation analysis to calculate the propagation velocity of AE signals (Li et al. 2018, Wang et al. 2021), designed waveform-based AE source localization algorithms (Li et al. 2020, Deng et al. 2021, Li et al. 2021,Wang et al. 2021), and distinguished AE signal characteristics corresponding to different damage types in terms of

frequency and the effect of water content on AE signal propagation (Li et al. 2020).

From the perspective of wave propagation, the AE signal contains at least two basic forms of longitudinal and transverse waves. According to the elastic wave theory, even for ideal surface waves, the transverse wave components have at least two modes, SV and SH. Moreover, the propagation speed of longitudinal waves is obviously faster than that of transverse waves, so the arrival moment of longitudinal waves is easier to identify, and the AE longitudinal waves are more valuable to study in terms of complexity and identification methods.

In this paper, considering the influence of different tree materials, *Zelkova schneideriana and Pinus sylvestris var. mongolica* specimens were selected as the research objects, and the AE source was generated by means of breaking a pencil lead and sending different pulse strings to study the propagation characteristics of AE longitudinal waves along the grain direction, mainly including the waveform characteristics, frequency distribution, propagation velocity and energy decay law of AE signal. Finally, the relationship among the time-frequency domain characteristics of AE longitudinal wave, wave velocity and Young's modulus of elasticity of wood were further explored.

MATERIALS AND METHODS

Experimental materials

In order to compare the propagation characteristics of AE signals in coniferous and broad trees, air-dried *Zelkova schneideriana (ZS)* and *Pinus sylvestris (PS)* specimens were selected as the subjects of the study. Considering the effective propagation distance of AE signal, the specimens of 800 mm (length) × 100 mm (width) × 30 mm (thickness) were made respectively, and it was ensured that the specimens were free from defects and the texture was straight. The densities of ZS and PS specimens were 0.696 $g \cdot cm^{-3}$ and 0.465 $g \cdot cm^{-3}$, and the moisture contents were 14.3% and 11.1%, resp. In order to verify the relationship between AE longitudinal wave velocity and Young's modulus of elasticity, small specimens were made into dumbbell-type specimens with reference to GB/T 1938: 2009, and the corresponding Young's modulus of elasticity was tested by tensile test on Shimadzu AG-X100kN electronic universal material testing machine.

The AE signal is dynamically acquired by a 5 channel high-speed data acquisition system, in which the data acquisition device is NI USB-6366 high-speed data acquisition card, and the sensor is an AE sensor of Songhua SR-150N with a resonant frequency of 150 kHz, the gain of its PAI front-end amplifier is 40 dB, the frequency is set to 500 kHz, and the AE signal amplitude range is (-5V, 5V). The AE sensor acquires and stores the AE signal in the LabVIEW environment, and the AE signal time-frequency domain characteristics is further analyzed in the MATLAB environment in the later stage. To enhance the energy of the AE source, a Dingyang SDG 805 signal generator was used to send out pulse strings with different voltage levels.

Methods

Five AE sensors were arranged at equal spacing of 150 mm on a plane of 800 mm × 100 mm in the specimen, and the AE source was simulated by breaking a pencil lead and sending pulse

strings generated by the signal generator in a plane of 100 mm × 30 mm, and the AE sensors and AE source were always kept in the same plane and the same line during the test. To prevent distortion of the sensor signal closest to the AE source, and ensured that the AE source could reach the farthest sensor, it was determined that the lead was broken and the pulse string was sent at a distance of 100 mm from the first AE sensor. The pencil lead breaking test was performed according to ASTM E976-2015. A 40 mm long, 0.5 mm pencil lead was used for the fracture test, and placed at 30° to the surface of the specimen and broken at a distance of 2.5 mm from the contact point. In the study of the AE energy decay law, a pulse string with the resonant frequency (150 kHz) of the AE sensor was generated by the signal generator, and the number of the pulse strings was set to 10000 and the voltages were set to 20 V, 15 V, 10 V and 5 V, resp. The pulse strings were sent through the AE sensor (Fig. 1). The actual test setup and sensor arrangement are shown in Fig.1a.

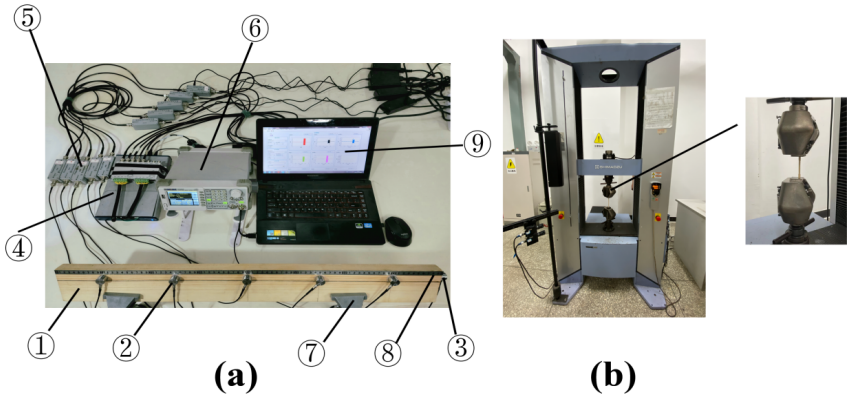

① Specimen; ② AE sensor; ③ AE sensor; ④ USB-6366 acquisition card; ⑤ front-end amplifier; ⑥ SDG 805 signal generator; ⑦ fixed fixture; ⑧ scale; ⑨ AE signal acquisition interface, where sensor ③ is connected to signal generator ⑥ for sending a 150 kHz pulse string.

Fig. 1: Test device and composition: a) AE signal acquisition system, b) tensile test.

According to the elastic wave theory, the propagation velocity of longitudinal waves in materials is significantly higher than that of transverse waves (Wang et al. 2021), so the first to reach the AE sensor must be the longitudinal wave component. When the first wave time difference method is used to calculate the AE longitudinal wave propagation velocity, the specific practice is to first determine the first arrival time of the AE signal according to the time domain waveform, and then calculate the time difference of the AE signal passing through different sensors, and then the ratio of distance to time difference is used as the AE signal propagation velocity. In the analysis of the AE signal energy, the AE signal is considered as an AC current and the heat generated through a 1Ω resistor at a fixed time is taken as the AE signal energy.

$$W = \int_0^t \frac{u^2}{R} d\tau \# \quad (1)$$

Since the AE signal collected by the system is discontinuous, for this reason Eq. 1 is discretized with $1/f_s$ seconds between two data, assuming that the discretization process uses a zero-order retainer, that is, the signal amplitude remains constant during this time, so the AE signal energy is calculated as:

$$W = \sum_{i=1}^{n} \Delta t_i \cdot u_i^2 = nT \sum_{i=1}^{n} u_i^2 \# \quad (2)$$

$$\Delta t_i = T = 1/f_s \qquad i = 1,2,...,n$$

where: f_s is the sampling frequency and n is the data length.

RESULTS AND DISCUSSION

AE signal longitudinal wave time-frequency characteristics

Pencil lead breaking can simulate the burst AE signal source, which is close to the ideal pulse signal with a wide frequency range, and is the most commonly used method to generate artificial AE source. It is also widely used in the research work related to wood AE. Considering the randomness of pencil lead breaking, 15 independent lead breaking tests were conducted at the same position of each specimen, and the waveform of 5 AE sensors in each lead breaking test were recorded. Fig. 2 shows the 5 sets of AE signal waveform of one lead breaking test for two specimens, and the other lead breaking tests all generate similar AE signal waveform.

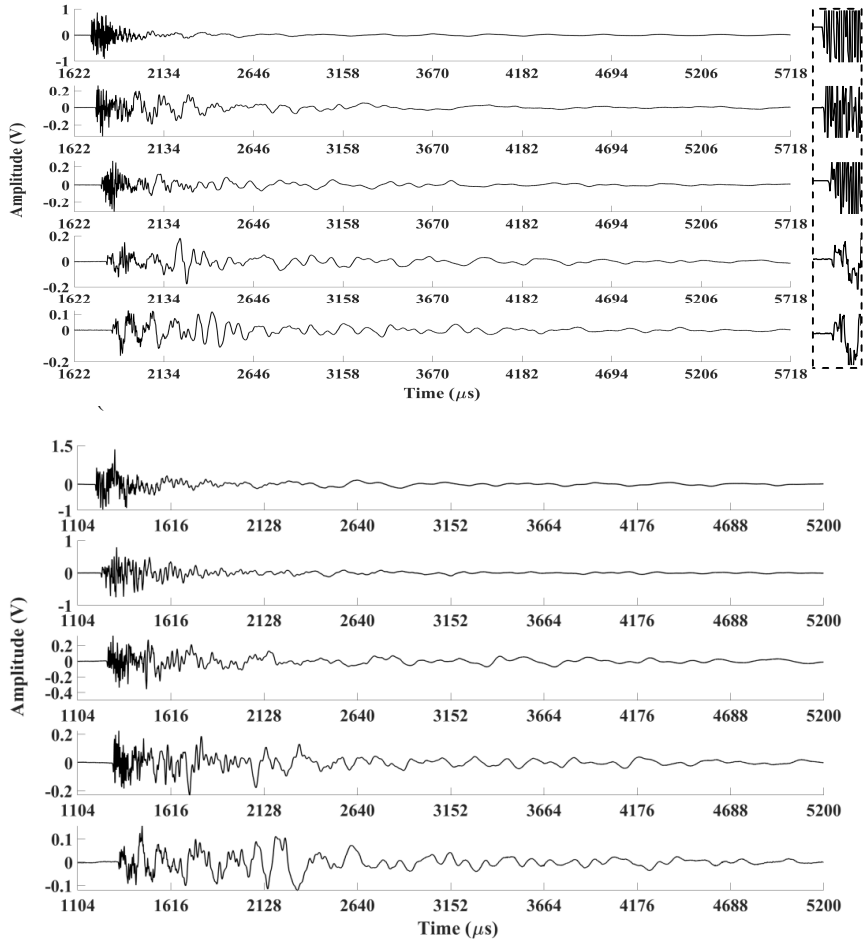

Fig. 2: AE waveform of two test specimens: (a) Z. schneideriana, (b) P. sylvestris.

In each group of waveforms in Fig. 2, the five AE sensor waveform from the nearest to the farthest AE source location are shown from top to bottom. The waveform in the dashed box

on the right side of Fig. 2a are local zooms corresponding to each AE waveform, and it can be seen from this local zoom that the AE longitudinal waveform all produce significant amplitude mutations when they reach the sensor, thus facilitating the determination of the arrival time of the first wave. To facilitate waveforms display as well as frequency domain analysis, 2048 data were intercepted for each waveform starting from the same time. Since the sampling frequency is 500 kHz, that is, the data interval is 2 μs, the time length of the whole waveform is 4096 μs, and the starting positions 1622 μs and 1104 μs in the abscissas of Fig. 2 represent the time when the AE waveform starts to be intercepted.

It can be seen from Fig. 2 that although the pencil lead breaking duration is very short, the lengths of the five AE waveform are all around 4 ms. It is worth noting that the waveform amplitude decreases significantly from near to far and the frequency is higher when the longitudinal signal just arrives, and after a shorter time (around 500 μs), the five AE waveform appear at a lower frequency with comparable amplitude and similar waveform. According to the elastic wave theory, the high-frequency components in the AE longitudinal wave will decay rapidly, while the low-frequency components will not be easily decayed and will be continuously reflected in the specimen to form a standing wave. Theoretically, the amplitude of the standing wave, formed by the superposition of two rows of traveling waves with opposite propagation directions and the same frequency, remains unchanged. But due to the porous media properties of wood, the AE longitudinal waves of any frequency will be significantly attenuated, so the second half of the waveform in Fig. 2 reflects the nature of standing waves, i.e., the vibration waveform collected at different locations are similar. For this reason, two segments signal of the waveform from Fig. 2 are taken out to frequency analysis. The first segment signal is the 256 data after the arrival of the first wave, i.e., a 512 μs long segment of the waveform starting from the first wave, which is regarded as the AE signal; the second segment signal is the 1024 data after the end of the previous AE signal, i.e., a 2048 μs long segment of the waveform, which is regarded as the standing wave signal.

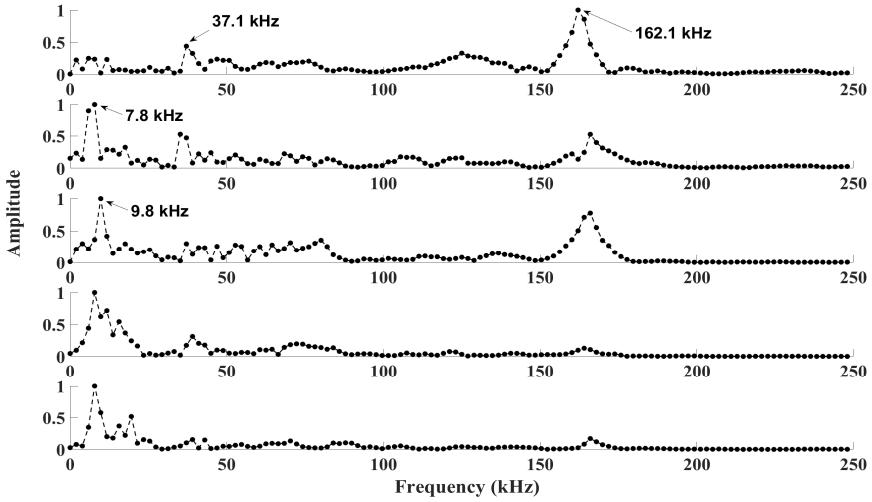

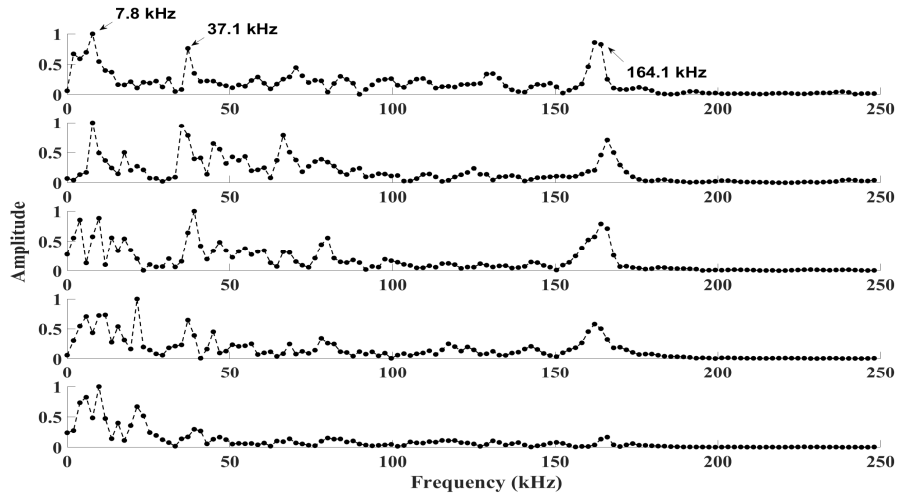

Fig. 3: AE signal spectrum: (a) Z. schneideriana, (b) P. sylvestris.

Fig. 3 shows the spectrum diagrams of these two segments' signal in the two specimens. For comparison, the corresponding spectra are normalized so that the main frequency components of the signals can be more easily seen. In the analysis of the standing wave components, the abscissas of Fig. 4 are set in the range of 0-20 kHz because only the fundamental frequency of the standing wave is concerned.

As shown in Fig. 3, since both AE sources are generated by breaking the pencil lead and the longitudinal waves are propagated along the fiber direction, the AE frequency components of the two specimens are basically the same, and the high-frequency component at 164 kHz is significantly attenuated, and there is almost no corresponding frequency component in the *ZS* specimen of the fourth sensor at a distance of 550 mm from the AE source, compared with the relatively longer propagation distance of the *PS* specimen. In contrast, the *PS* specimen propagates at a relatively longer distance, and the frequency components around 37 kHz have a similar decay pattern, while the relatively low frequency (7.8 kHz) components are not very significantly decayed. Such phenomenon is consistent with the basic theory of elastic waves. As for the difference in propagation distance between *ZS* and *PS*, it is mainly because the fibers of *PS* are longer than those of *ZS* , so the decay of the signal at the same frequency is relatively slower.

It can be seen from Fig. 4 that the fundamental frequencies of the standing wave components of the AE longitudinal waves are basically the same. Although the fundamental frequencies are shifted somewhat in some signals due to the measurement noise and the frequency response characteristics of the sensors, it can still be seen that the fundamental frequency of the standing wave of *ZS* is around 3.2 kHz and that of *PS* is around 2.9 kHz.

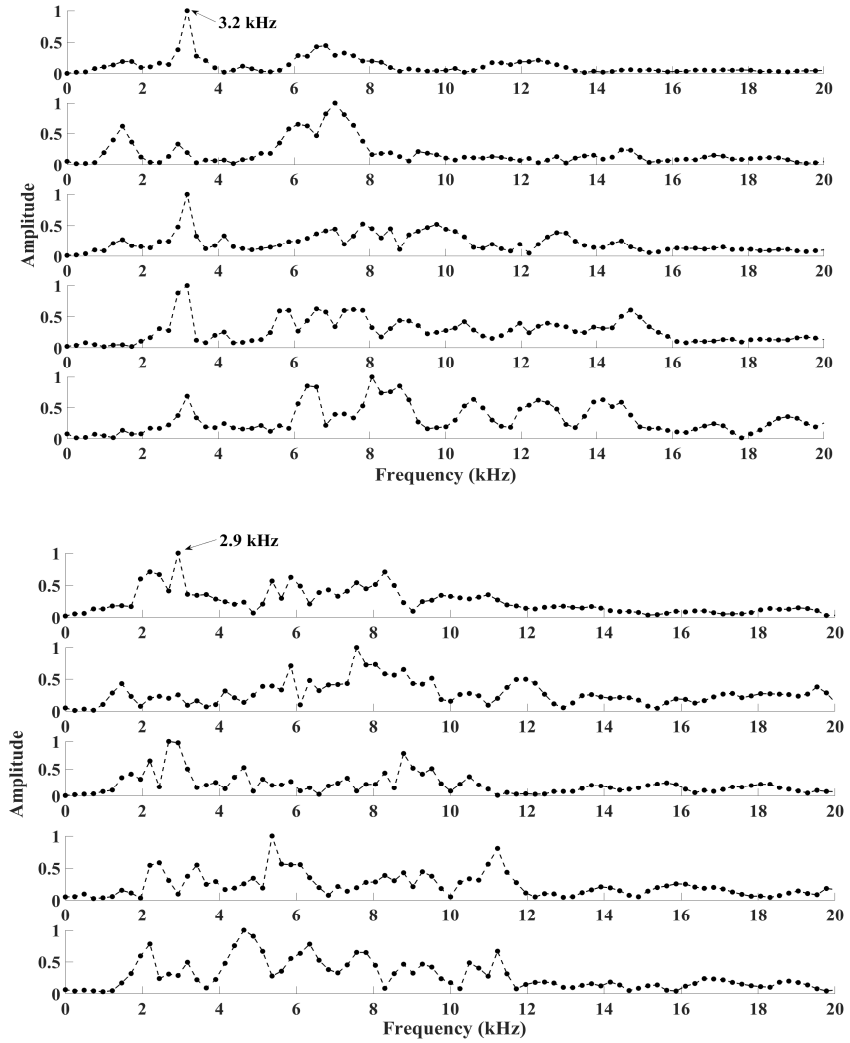

Fig. 4: Standing wave spectrum of AE signal: (a) Z. schneideriana, (b) P. sylvestris.

Propagation velocity of AE signal longitudinal wave

On the basis of Fig. 2, the propagation velocity of AE signal longitudinal wave can be calculated more easily by using the first wave time difference method, and the AE longitudinal velocities of the two specimens based on different distances are listed in Tab. 1. In the table, D1, D2, D3 and D4 correspond to the calculated velocities of 150 mm, 300 mm, 450 mm and 600 mm. The V_{av} in the last line represents the corresponding average velocity. It can be seen in Tab. 1 that the calculated velocities obtained from distances D1, D2 and D3 fluctuate significantly, mainly because the shorter the distance the greater the absolute error in velocity produced in the same time error. Therefore, in order to minimize the calculation error, the longest 600 mm distance was used to calculate the longitudinal wave velocity, and the propagation velocities of AE longitudinal wave *ZS* and *PS* specimens were 4959 $m \cdot s^{-1}$ and 4749 $m \cdot s^{-1}$ respectively.

Tab. 1: Propagation velocity of longitudinal waves in the two specimens.

	Zelkova schneideriana				*Pinus sylvestris*			
Time	D1 (mm)	D2 (mm)	D3 (mm)	D4 (mm)	D1 (mm)	D2 (mm)	D3 (mm)	D4 (mm)
s	v_1 (m.s^{-1})	v_2 (m.s^{-1})	v_3 (m.s^{-1})	v_4 (m.s^{-1})	v_1 (m.s^{-1})	v_2 (m.s^{-1})	v_3 (m.s^{-1})	v_4 (m.s^{-1})
1	5357	5000	5357	4762	5357	3947	5769	4839
2	4412	5769	4167	4688	5357	4167	4688	4839
3	5000	5769	4688	5085	4688	4688	4688	4688
4	4688	5000	5357	4918	5000	4412	4688	4688
5	5357	5000	4688	5000	4688	5357	5769	4839
6	5357	5357	5000	5085	4688	4688	4688	4688
7	6250	5000	4688	5126	5000	4412	4167	4545
8	5357	4688	5769	4839	5769	4412	4167	4688
9	5357	5000	4688	4686	5357	3947	5000	4839
10	5357	4412	4688	4762	4688	4688	4688	4688
11	5357	5000	4688	5000	4688	4688	4688	4688
12	5000	5769	4688	5085	5000	4412	4688	4688
13	6250	5000	4688	5172	4688	5357	5769	4839
14	6250	5000	4688	5172	5357	3947	5769	4839
15	5357	5000	4688	5000	5357	4688	5769	4839
V_{av}	5382	5126	4846	**4959**	5045	4521	4999	**4749**

According to the elastic wave theory, the propagation velocity of the longitudinal wave depends on the material itself, i.e., it is determined by the Young's modulus of elasticity and density of the material. So the Young's modulus of elasticity of the material can be calculated based on the velocity of the AE longitudinal wave. In addition, from the principle of standing wave generation, its fundamental frequency is mainly determined by the length of the specimen and the velocity of the traveling wave, i.e.:

$$c_p = 2lf \tag{3}$$

where: c_p is the velocity of the traveling wave generating standing wave; l is the length of the specimen; f is the fundamental frequency of the standing wave.

From the fluctuation propagation equation based on a one-dimensional rod, when the elastic deformation in the vertical propagation direction is not considered, i.e., when the Poisson's ratio of the material is defaulted to zero, the relationship between the longitudinal wave velocity and Young's modulus of elasticity is as follow:

$$c_p = \sqrt{E / \rho} \tag{4}$$

where: E is the Young's modulus of elasticity; ρ is the density of the specimen.

To investigate the relationship among the AE longitudinal velocity, Young's modulus of elasticity and the fundamental frequency of the standing wave, a dumbbell-shaped tensile specimen were intercepted from different parts of the two specimens and tested on a universal material testing machine (Fig. 1b) to test the Young's modulus of elasticity of the material, and the corresponding

results are shown in Tab. 3. In Tab. 2, E_1 is the actual measured Young's modulus of elasticity; E_2 is the calculated Young's modulus of elasticity based on the calculated longitudinal wave velocity according to Eq. 4; c_p is the AE longitudinal wave velocity calculated according to the first wave time difference method; v is the Poisson's ratio of the material; f_{sw} is the standing wave fundamental frequency obtained from the previous analysis; C_p is the AE longitudinal wave velocity calculated according to the fundamental frequency and Eq. 3.

Tab. 2: Comparison table of measurement and calculation results.

Specimen	ρ (g·cm^{-3})	E_1 (GPa)	E_2 (GPa)	c_p (m·s^{-1})	ν	f_{sw} (kHz)	C_p (m·s^{-1})
Zelkova schneideriana	0.696	12.4	17.1	4959	0.308	3.2	5120
Pinus sylvestris	0.465	9.4	10.5	4749	0.203	2.9	4640

As shown in Tab. 2, the Young's modulus of elasticity calculated according to the actual AE longitudinal wave velocity is higher than the value obtained from the test, which is due to the premise of Eq. 4. The elastic deformation in the vertical propagation direction is ignored, that is, the Poisson's ratio of the material is considered to be zero. So the calculated Young's modulus of elasticity modulus is larger. According to the elastic wave theory, the propagation velocity of the longitudinal wave is expressed as Eq. 5:

$$c_p = \sqrt{\frac{\lambda + 2\mu}{\rho}} \tag{5}$$

where: λ and μ are the Lamé constants of the material, which are related to the Young's modulus of elasticity and Poisson's ratio of the material as Eq. 6 and Eq. 7:

$$\lambda = \frac{vE}{(1+v)(1-2v)} \tag{6}$$

$$\mu = \frac{E}{2(1+v)} \tag{7}$$

where: v is the Poisson's ratio of the material. From Eqs. 5-7, Eq. 8 can be deduced.

$$\frac{c_p^2 \rho}{E} = \frac{1-v}{(1+v)(1-2v)} \tag{8}$$

Letting

$$\alpha = \frac{c_p^2 \rho}{E} \tag{9}$$

The equation for calculating Poisson's ratio can be obtained as Eq. 10:

$$2\alpha v^2 + (\alpha - 1)v + (1-\alpha) = 0 \tag{10}$$

When the longitudinal wave velocity and Young's modulus of elasticity E_1 measured by the test were brought into the Eq. 10, the Poisson's ratios of 0.308 and 0.203 for *ZS* and *PS specimens* can be respectively obtained. Because the measurement of Poisson's ratio of wood is complicated and the error is large, so no relevant test is made in this paper, but the calculated Poisson's ratio is consistent with the existing Poisson's ratio of wood. The above derivation also further shows that the

Young's modulus of elasticity calculated based on Eq. 4 is obviously larger due to the Poisson's ratio of the material is neglected, which is obviously prone to large errors for the application of AE NDT techniques in wood.

The last column of Tab. 2 shows that the propagation velocities of longitudinal waves in *ZS* and *PS* specimens calculated by standing wave fundamental frequency are 5120 $m \cdot s^{-1}$ and 4640 $m \cdot s^{-1}$, and the respective relative errors are 3.2% and 2.3% compared with the experimentally measured longitudinal velocities, thus indicating that the propagation velocity of longitudinal waves can be estimated more accurately by the standing wave fundamental frequency of AE longitudinal waves.

Energy decay law of AE signal longitudinal wave

As shown in Fig. 2, AE signal attenuates obviously in the process of propagation, and it is difficult to be used directly to analyze the energy decay process of the longitudinal wave because of the limited energy of the AE source generated by the pencil lead breaking and the obvious standing wave signal that will be generated. For this reason, in this paper, an AE sensor ③ (Fig. 1) is used as the source signal, and a pulse string of length 10000 at 150 kHz is sent through the signal generator to ensure that each sensor can receive the pulse strings from the source, and the AE signal energy at different locations is calculated according to Eq. 2. The results are shown in Tab. 4, where U is the amplitude of the pulse strings in V; E1-E5 denote the AE signal energy received by the five AE sensors from near to far, and the unit is μJ.

Tab. 3: AE signal energy distribution table.

Specimen	*U* (V)	E1 (μJ)	E2 (μJ)	E3 (μJ)	E4 (μJ)	E5 (μJ)
Zelkova schneideriana	20	99.054	1.813	0.535	0.190	0.035
	15	56.223	1.049	0.307	0.108	0.019
	10	24.666	0.471	0.136	0.048	0.009
	5	6.173	0.118	0.034	0.012	0.002
Pinus sylvestris	20	95.407	12.022	2.239	0.585	0.037
	15	54.017	6.978	1.269	0.338	0.019
	10	23.863	3.144	0.564	0.152	0.008
	5	5.812	0.817	0.142	0.041	0.002

As can be seen from Tab. 3, the AE signal energy of the sensor closest to the AE remains consistent at different voltage levels even in different materials specimens, but the energy undergoes significant decay as the propagation distance increases. In order to reflect the decay process of AE energy more intuitively, the AE longitudinal energy of different voltage levels is plotted as a line in the same figure, as shown in Fig. 5.

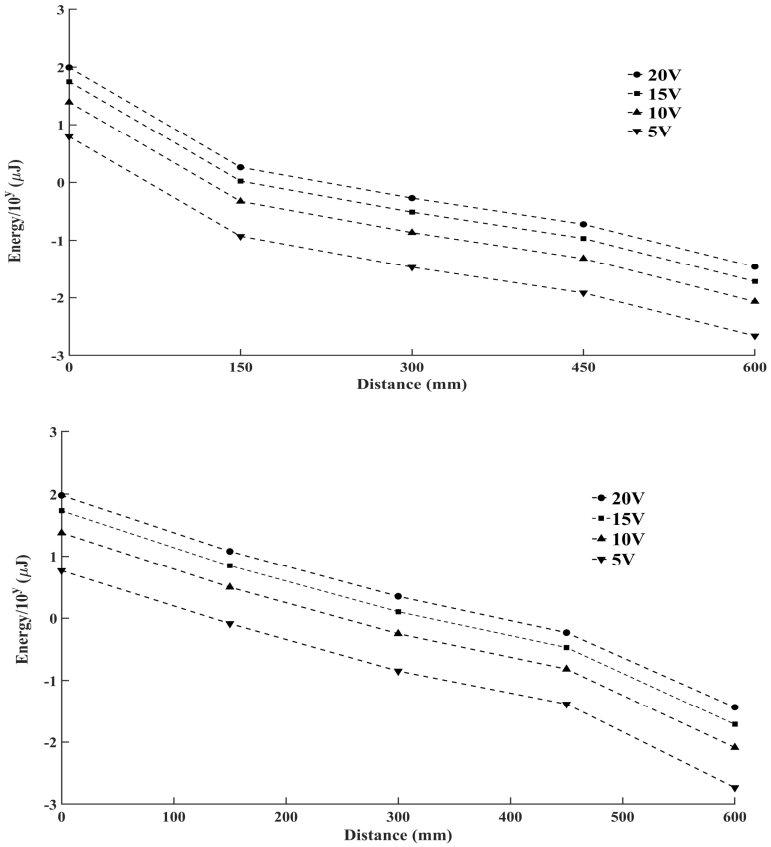

Fig. 5: AE longitudinal wave energy distribution: (a) Z. schneideriana, (b) P. sylvestris.

Since the energy of AE longitudinal wave varies too much, the ordinate in Fig. 5 is the value after the energy is taken logarithmically. It can be intuitively seen from Fig. 5 that although the voltage levels are different, i.e., the energy of AE source is different, the decay law of energy is basically the same in the same specimen. For this reason, in this paper, the AE longitudinal energy is the decay process of exponential fitting, and the AE longitudinal energy measured by the sensor closest to the AE source is considered as 1, and the AE longitudinal energy at other locations is normalized, and the fitting curve is shown in Fig. 6.

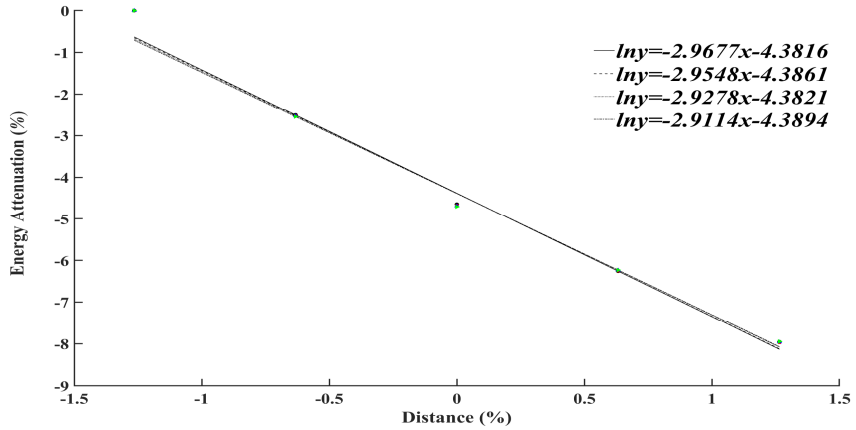

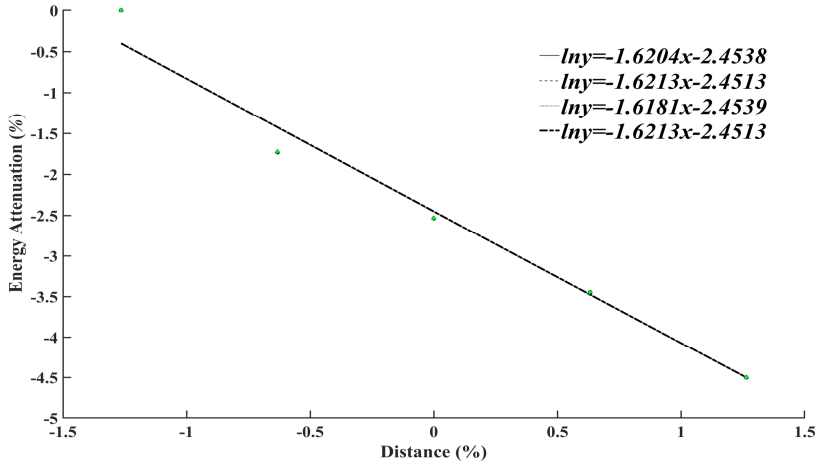

Fig. 6: AE longitudinal wave energy attenuation fitting curve: (a) Z. schneideriana, (b) P. sylvestris.

When considering the decay law of AE longitudinal wave energy with distance, direct fitting is prone to large fitting errors due to the significant difference between the logarithm of energy and distance. So the following centered linear treatment of distance is performed.

$$x = \frac{D - mean(D)}{std(D)} \tag{11}$$

where: D is the actual distance, taken in the range of 0~600 mm; x is the transformed equivalent distance, i.e., the horizontal axis coordinates in Fig. 6; *mean*(D) is the expectation of D; *std*(D) is the variance of D.

In this paper, the expectation and variance are 300 mm and 173.638 mm respectively. The attenuation law of AE longitudinal wave in *ZS* specimen with distance obtained from the fit of Fig. 6a is obtained as Eq. 12:

$$E = e^{-2.94x - 4.38} \tag{12}$$

The decay law of AE longitudinal waves in *PS* specimen with distance obtained from the fit of Fig. 6b is obtained as Eq. 13:

$$E = e^{-1.62x - 2.45} \tag{13}$$

Bringing Eq. 11 into the above two equations respectively, the attenuation functions of AE longitudinal waves with distance in *ZS* specimen and *PS* are obtained as follow.

$$E_{ZS} = 2.0128e^{-0.0168D} \tag{14}$$

$$E_{PS} = 1.4175e^{-0.0093D} \tag{15}$$

It is obvious from Eq. 14 and Eq. 15 that the AE longitudinal wave decays faster in *ZS* specimen, and based on the energy decay to 50%, the AE longitudinal wave propagation distance

in *ZS* and *PS* is 85 mm and 112 mm, respectively. Li et al. (2021) showed that the attenuation indices of internal longitudinal waves were -0.1157 and -0.009561, which are consistent with the results of this paper.

CONCLUSIONS

In this paper, the propagation characteristics and energy decay law of the longitudinal wave of AE signal in the grain direction of the wood were studied, and the interrelationship among the longitudinal wave velocity, Young's modulus of elasticity, and standing wave fundamental frequency was studied, and the following main conclusions were obtained: *(1)* In the process of propagation, the high frequency components of the longitudinal wave appear obvious attenuation, and the longitudinal wave components with lower frequency will form obvious standing wave phenomenon under the effect of continuous reflection. *(2)* Using the fundamental frequency of the standing wave component, the velocity of the longitudinal wave can be estimated more accurately. For the two specimens in this paper, the relative error of the estimated velocity of the standing wave fundamental frequency is only 3.2% and 2.3%. *(3)* Based on the velocity of AE longitudinal wave obtained by experiment, the Young's modulus of elasticity of wood can be calculated by Eq. 4, but the calculated modulus of elasticity is obviously larger, so the Poisson's ratio of the material needs to be considered when applying the longitudinal wave velocity to derive the Young's modulus of elasticity of wood. *(4)* The AE signal energy showed an obvious exponential decay with the increasing of propagation distance. Since the longitudinal waves in the grain direction propagate mainly along the fibers, the AE signal energy decayed faster in *Zelkova schneideriana* with shorter fibers.

ACKNOWLEDGEMENTS

The authors are grateful for the support of the China Natural Science Foundation (NO: 32160345, 31760182) and Department of Education of Yunnan Provincial (NO: 2021J0156, NO: 2021J0158), Start up fund for introducing talents and scientific research of Anhui University of Engineering (NO: 2021YQQ037).

REFERENCES

1. Aicher, S., Hofflin, L., Langer, G.D, 2001: Damage evolution and acoustic emission of wood at tension perpendicular to fiber. Holz als Roh- und Werkstoff 59: 104-116.
2. Berg, J.E., Gradin, P.A., 2000: Effect of temperature on fracture of spruce in compression, investigated by use of acoustic emission monitoring. Journal of Pulp and Paper Science 26(8): 294-299.
3. Chen, Z., Gabbitas, B., Hunt, D., 2006: Monitoring the fracture of wood in torsion using acoustic emission. Journal of Materials Science 41: 3645-3655.
4. Contea, S.L., Vaiedelicha, S., Thomas, J.H., Muliavac, V., Reyer, D., Maurind, E, 2015: Acoustic emission to detect xylophagous insects in wooden musical instrument. Journal of Cultural Heritage 16: 338–343

5. Deng, T.T., Ju, S., Wang, M.H., Li, M., 2021: Study on propagation law of acoustic emission signals on anisotropic wood surface. Wood Research 66(4): 517-527.
6. Fang S.Y., Qiu, R.Z., Li, M., 2018: Characterization of wood acoustic emission signals based on improved EMD algorithm. Vibration and Shock 37(23): 292-298.
7. Guo, X.L., Guo, Y., Hu, W., Cao, P.X., 2011: Study of acoustic emission characteristics of wood matrix composites during damage. Journal of Nanjing Forestry University: Natural Science Edition 35(3): 97-100.
8. Krauss, A., Kudela, J., 2011: Ulrasonic wave propagation and Young's modulus of elasticity along the grain of Scots pine wood (*Pinus sylvestris* L.) varying with distance from the pith. Wood Research 56(4): 479-488.
9. Lamy, F., Takarli, M., Angellier, N., Dubois, Pop, O., 2015: Acoustic emission technique for fracture analysis in wood materials. International Journal of Fracture 192(1): 57-70.
10. Li, M., Wang, M.H., Deng, T.T., Fang, S.Y., Lai, F., Luo R.H., 2021: Study of acoustic emission propagation characteristics and energy attenuation of surface transverse wave and internal longitudinal wave of wood. Wood Science Technology 55: 1619–1637.
11. Li, X.C., Ju, S., Luo, T.F., Li, M., 2020: Effect of moisture content on propagation characteristics of acoustic emission signal of *Pinus massoniana* lamb. European Journal of Wood and Wood Products 78: 185-191.
12. Li, X.S., Deng, T.T., Wang, M.H., Ju, S., Li, X.C., Li, M., 2020: Improvement of linear localization algorithm for wood acoustic emission sources based on wavelet and correlation analysis. Journal of Forestry Engineering 5(3): 138-143.
13. Li, X.S., Deng, T.T., Wang, M.H., Li, M., 2021: Localization of acoustic emission source on glulam surface based on signal similarity wavelet reconstruction. Journal of northwest forestry university 36(2): 202-207.
14. Li, Y., Yu, S.S., Dai, L., Luo, T.F. , Li, M., 2018: Acoustic emission signal source localization on plywood surface with cross-correlation method. Journal of Wood Science 64(2): 78-84.
15. Nasir, V., Cool, J.., 2020: Characterization, optimization, and acoustic emission monitoring of airborne dust emission during wood sawing. International Journal of Advanced Manufacturing Technology 109: 2365-2375.
16. Nasir, V., Nourian, S., Avramidis, S., 2019: Stress wave evaluation by accelerometer and acoustic emission sensor for thermally modified wood classification using three types of neural networks. European Journal of Wood and Wood Products 77(1): 45-55.
17. Niemz, P., Brunner, A.J., Walter, O., 2009: Investigation of the mechanism of failure behaviour of wood based materials using acoustic emission analysis and image processing. Wood Research 54(2): 49-62.
18. Ohuchi, T., Hermawan, A., Fujimoto, N., 2011: Basic studies on fracture toughness of sugi and acoustic emission. Journal-Faculty of Agriculture Kyushu University 56(1): 99-102.
19. Reiterer, A., Tschegg, S.E.S., Tschegg, E.K., 2000: Mode I fracture and acoustic emission of softwood and hardwood. Wood Science and Technology 34: 417-430.
20. Sun, J.P., Wang, F.H., Zhu, XD, Yan, LQ., 2006: Detection of damage processes in poplar wood based on acoustic emission under dynamic loading. Forestry Science 42(9): 89-92.

21. Shao, Z.P., Chen P., Zha C.S., Ji, K., 2009: Acoustic emission characteristics and Felicity effect of wood damage fracture process. Forestry Science 45(2): 86-91.
22. Wang, M.H., Li M., Deng T.T., Fang, S.Y., Li X.S., Lai, F., 2021: Study on lamb wave propagation characteristics along the grain of thin wood sheet. Wood Research 66(1): 141-152.
23. Wang, M.H., Deng, T.T., Li, X.S., Ding R, Lai, F., Luo, R.H., Li, M., 2021: propagation characteristics of acoustic emission signal L-Shaped wood. Journal of northwest forestry university 36(2): 213-219.
24. Wu, Y., Shao Z.P., Wang, F., Tian, G.L .,2014: Acoustic emission characteristics and Felicity effect of wood fracture perpendicular to the grain. Journal of Tropical Forest Science 26(4):522-531.
25. Yang, Z., Jiang, Z., Hse C.Y., Liu, R.,2017: Assessing the impact of wood decay fungi on the modulus of elasticity of slash pine (*Pinus elliottii*) by stress wave non-destructive testing. International Biodeterioration & Biodegradation 117: 123–127.

SAIYIN FANG, TINGTING DENG, KUN DU
SOUTHWEST FORESTRY UNIVERSITY
SCHOOL OF MACHINERY AND TRANSPORTATION
BAILONG ROAD 300, PANLONG DISTRICT
KUMMING
CHINA

MING LI*
[1]KEY LABORATORY OF ADVANCED PERCEPTION AND INTELLIGENT CONTROL OF HIGH-END EQUIPMENT OF MINISTRY OF EDUCATION
[2]ANHUI POLYTECHNIC UNIVERSITY
WUHU
CHINA
*Corresponding author: swfu_lm@swfu.edu.cn